optica

Quantum frequency conversion of a quantum dot single-photon source on a nanophotonic chip

Anshuman Singh,[1,2,8] Qing Li,[1,2] Shunfa Liu,[3] Ying Yu,[3] Xiyuan Lu,[1,2] Christian Schneider,[4] Sven Höfling,[4,5] John Lawall,[1] Varun Verma,[6] Richard Mirin,[6] Sae Woo Nam,[6] Jin Liu,[3,9] and Kartik Srinivasan[1,7,*]

[1]National Institute of Standards and Technology, Gaithersburg, Maryland 20899, USA
[2]Maryland NanoCenter, University of Maryland, College Park, Maryland 20742, USA
[3]State Key Laboratory of Optoelectronic Materials and Technologies, School of Electronics and Information Technology, School of Physics, Sun-Yat Sen University, Guangzhou, China
[4]Technische Physik, Universität Würzburg, D-97074 Würzburg, Germany
[5]SUPA, School of Physics and Astronomy, University of St Andrews, St Andrews, UK
[6]National Institute of Standards and Technology, Boulder, Colorado 80305, USA
[7]Joint Quantum Institute, NIST/University of Maryland, University of Maryland, College Park, Maryland 20742, USA
[8]e-mail: anshuman.singh@nist.gov
[9]e-mail: liujin23@sysu.edu.cn
*Corresponding author: kartik.srinivasan@nist.gov

Received 16 January 2019; revised 28 March 2019; accepted 28 March 2019 (Doc. ID 357890); published 30 April 2019

Single self-assembled InAs/GaAs quantum dots are promising bright sources of indistinguishable photons for quantum information science. However, their distribution in emission wavelength, due to inhomogeneous broadening inherent to their growth, has limited the ability to create multiple identical sources. Quantum frequency conversion can overcome this issue, particularly if implemented using scalable chip-integrated technologies. Here, we report the first demonstration to our knowledge of quantum frequency conversion of a quantum dot single-photon source on a silicon nanophotonic chip. Single photons from a quantum dot in a micropillar cavity are shifted in wavelength with an on-chip conversion efficiency ≈12%, limited by the linewidth of the quantum dot photons. The intensity autocorrelation function $g^{(2)}(\tau)$ for the frequency-converted light is antibunched with $g^{(2)}(0) = 0.290 \pm 0.030$, compared to the before-conversion value $g^{(2)}(0) = 0.080 \pm 0.003$. We demonstrate the suitability of our frequency-conversion interface as a resource for quantum dot sources by characterizing its effectiveness across a wide span of input wavelengths (840–980 nm) and its ability to achieve tunable wavelength shifts difficult to obtain by other approaches.

https://doi.org/10.1364/OPTICA.6.000563

1. INTRODUCTION

Single photons are fundamental constituents of many quantum technologies [1–5]. Self-assembled InAs/GaAs quantum dots (QDs) [6], in particular, have been steadily developed as single-photon sources [7,8] to the point that they can now outperform other sources in simultaneously achieving high brightness, single-photon purity, and indistinguishability [9–12]. As a result, they are relevant to applications that rely on quantum interference of single photons, including linear optics quantum computing [13] and more specialized simulations such as Boson sampling [14,15]. Recent Boson sampling experiments using a single QD single-photon source de-multiplexed into a waveguide interferometer network have shown promising potential to scale up the computational complexity that can be addressed in such experiments [16–18]. Further progress, not just on Boson sampling but also in other areas such as the construction of multi-photon entangled states, would be greatly aided by increasing the available photon flux through the ability to create multiple identical QD single-photon sources. However, the inhomogeneous broadening characteristic of self-assembled InAs/GaAs QDs [6] limits the extent to which any two QDs can be expected to have the same emission wavelength.

To generate identical photons from multiple QDs, one needs to overcome this spectral mismatch, and many different approaches have been considered. Strain [19], optical Stark shifts [20], and electrical Stark shifts [21] have been used to tune QD emission and enable interference of photons from different QDs [22–24] (Fig. 1). Through suitable engineering of the epitaxial growth layers or the device geometry surrounding the QD, the typical sub-nanometer wavelength shifts achievable by these approaches can be significantly increased to the ≈10 nanometer scale [25–28]. However, these approaches may not be compatible

with arbitrary photonic geometries, limiting the design space available when using such structures to achieve desired performance (e.g., in terms of Purcell enhancement, photon indistinguishability, and efficient collection into a desired optical channel). In contrast, quantum frequency conversion (QFC) [29,30] acts on the emitted photons rather than the QD energy levels, so that it can be applied to any arbitrary QD single-photon source geometry. QFC can achieve large spectral shifts, with upconversion [31] and downconversion [32,33] between telecom and near-visible photons emitted from QDs demonstrated in centimeter-scale, $\chi^{(2)}$ nonlinear waveguides. Along with their relatively large size and power consumption, such single-stage $\chi^{(2)}$ approaches necessitate large spectral shifts, and as a result both QD sources needed to be converted to a target wavelength far outside of the original band [34,35]. In contrast, here we use four-wave mixing Bragg scattering (FWM-BS) [36] in compact, power-efficient nanophotonic resonators [37] to perform intraband conversion suitable for spectrally shifting the photons over a range between 1.6 and 12.8 nm, an appreciable fraction of the QD ensemble inhomogeneous distribution. Furthermore, as the spectral translation range in FWM-BS is set by the difference in frequencies of two pump lasers, it can also produce large spectral shifts, including downconversion to the telecom band at the single-photon level [37]. FWM-BS thus provides a unique opportunity to cover an extremely large spectral translation range, including the gap between approaches that tune the QD energy levels and $\chi^{(2)}$ techniques (Fig. 1).

In Ref. [37], our focus was on establishing the device engineering to enable efficient, microresonator-based FWM-BS, and experiments were restricted to working with classical input signals created by attenuated, continuous-wave laser light. Here, we demonstrate true quantum frequency conversion of single-photon states produced by a QD. We study how the linewidth of the QD photons influences the achievable conversion efficiency due to the finite bandwidth of our frequency converter and the impact of frequency conversion on photon statistics. We also show how to tailor our frequency converter to work with a wide range of input wavelengths, of importance for addressing the inhomogeneous broadening of QDs on the same sample and across different wafer growths. Our results show the promise of integrated nanophotonics technology for quantum frequency-conversion applications, while also highlighting future directions for improving device performance with respect to the key metrics of conversion efficiency and added noise.

2. QFC USING FWM-BS

To date, FWM-BS has been applied to quantum states of light produced by spontaneous nonlinear processes in macroscopic crystals and fibers, with QFC taking place within optical fibers [38,39]. Here, we combine a nanophotonic quantum light source—a single InAs/GaAs QD in a micropillar cavity—with a nanoscale frequency converter based on efficient and low-noise FWM-BS in Si_3N_4 micorings [37], as schematically depicted in Fig. 2. This first demonstration of QFC of QD single photons via FWM-BS highlights the optical compatibility of the source and frequency converter. This is non-trivial, as the frequency-converter bandwidth must accommodate the source linewidth, while the temporal duration of the pumps that enable efficient frequency conversion must be longer than that of the single photon wavepackets. As described below, our microresonator-based frequency converter has a bandwidth on par with (and in some cases, significantly larger than) that of the photons generated by InAs/GaAs QDs [7,8], and it utilizes continuous-wave pumps (in contrast to picosecond and nanosecond pulses used in Refs. [38] and [39], respectively), suggesting that these compatibility requirements can be met. Moreover, the recent demonstration of heterogeneous integration of InAs/GaAs QD single-photon sources with Si_3N_4 nanophotonic circuits [40] suggests that source and converter can eventually be combined within a single integrated chip.

The two-pump nature of FWM-BS means that input signal photons at ω_s can be both frequency upshifted and downshifted, with the shift given by the difference in pump frequencies $(\omega_{p1} - \omega_{p2})$ as shown in the energy diagram in Fig. 2. The up- and downshifted fields are referred to as the blueshifted (ω_{i+}) and redshifted idlers (ω_{i-}), respectively. The conversion efficiency into each idler depends on the degree to which the four fields involved are frequency matched and phase matched [37]. For our devices, both blue- and re-detuned idlers are generated with nearly equal efficiency, with a single idler selected by bandpass filtering of the output light.

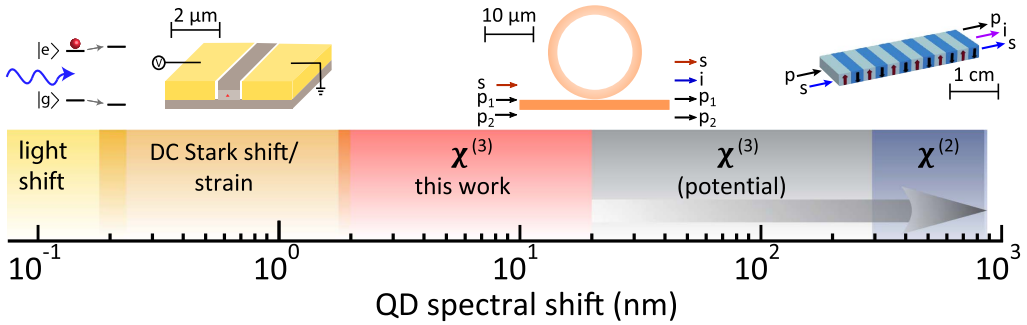

Fig. 1. Frequency shift techniques for quantum dots (QDs). Relatively small shifts are typically achieved by tuning the QD energy levels through optical fields (i.e., the light shift/AC Stark shift), strain, and electrical fields (DC Stark shift), as depicted on the left side of the image. The depicted ranges are typical results, but some engineered systems have produced significantly larger shifts [25–28]. Several hundred nanometer shifts have been obtained using quantum frequency conversion of the emitted photons in centimeter-scale $\chi^{(2)}$ nonlinear waveguides (right). Here, we implement four-wave mixing Bragg scattering, a $\chi^{(3)}$ non-linear process, in compact and power-efficient microring resonators, producing frequency shifts in an intermediate regime (red region) sufficient to cover the inhomogeneous broadening of QDs. Moreover, large spectral shifts can also be obtained through this process (gray area), enabling spectral shifts spanning from intraband to interband conversion (gray arrow).

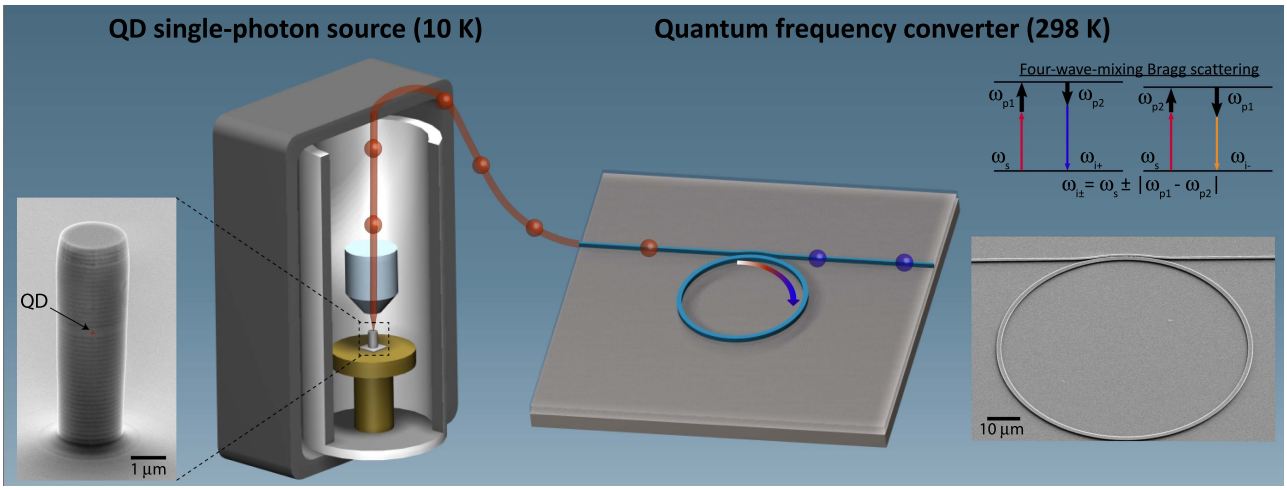

Fig. 2. Overview of the experiment. Single photons from the source chip (QD in a micropillar cavity housed in a 10 K cryostat) are out-coupled via optical fiber and sent to a frequency converter chip (microring resonator) operating at room temperature. An energy diagram depicting the four-wave mixing Bragg scattering process used for frequency conversion is shown in the top right, where two pumps (ω_{p1} and ω_{p2}) shift the input signal (ω_s) to idlers at frequencies ω_{i+} and ω_{i-}. The output of the frequency converter is a superposition of the remnant (unconverted) signal and the two idlers, with filtering used to select a specific spectral channel. Scanning electron microscope images of the single-photon source and frequency converter are shown on the left and right sides of the image, with the inferred location of the QD indicated.

3. SYSTEM DESIGN

Our microrings are fabricated in Si_3N_4, a material with low linear loss, appreciable nonlinearity, and negligible two-photon absorption at telecom wavelengths [41]. Our FWM-BS process involves two pumps in the telecommunications C band (1525–1565 nm) that convert an input signal at ≈ 917 nm to an output idler spectrally shifted between ≈1.6 nm and ≈12.8 nm from the input. The resonator cross section is chosen to ensure that the FWM-BS process is both phase matched and frequency matched; this is done by iterating between simulations that take into account material dispersion, waveguiding, and bending effects and experimental measurements of the cavity resonance positions using a wavemeter with specified 0.1 pm accuracy. We engineer the parameters of the coupling waveguide (waveguide width, gap with respect to the ring, and interaction length) to achieve overcoupling at the signal and idler wavelengths, and thus ensure that the majority of input signal photons are coupled into the resonator and the majority of frequency-converted idler photons are coupled back into the access waveguide. See Supplement 1 Sections VI and VII for more details.

4. QFC OF A QD SINGLE PHOTON SOURCE ON A NANOPHOTONIC CHIP

We first spectrally shift our QD source using the microring frequency converter. The QD is excited at its p shell at ≈903.31 nm using a tunable continuous-wave laser (see Supplement 1 Section I for info on the experimental setup and Section II for QD source fabrication). The QD spectrum has a single peak at ≈917.78 nm [Fig. 3(a)], and so we temperature tune the frequency converter to match this wavelength as discussed later in the context of Fig. 5(c). The QD emission is combined with two 1550 nm band pumps and sent into the microring converter, and the output spectrum of the converter shows a depleted QD signal that is accompanied by two dominant idlers: a blue idler at ≈916.17 nm and red idler at ≈919.39 nm [Fig. 3(b)].

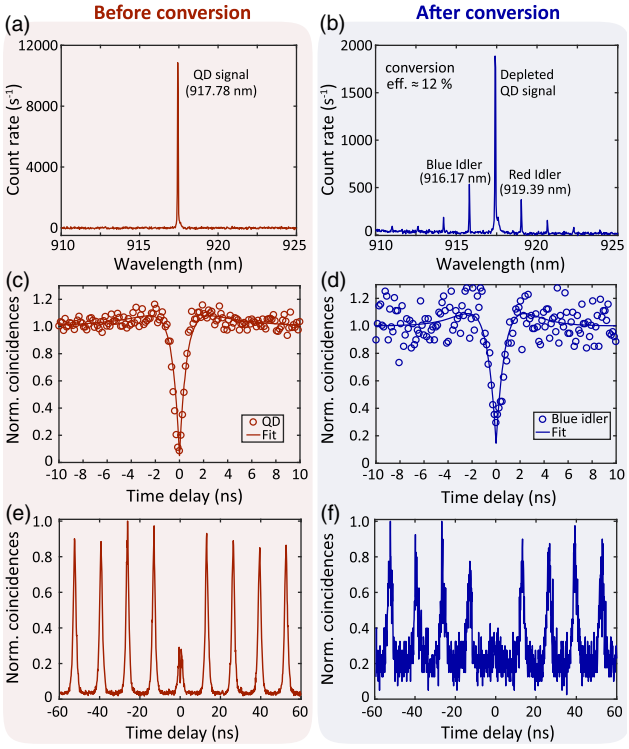

Fig. 3. Quantum frequency conversion of a QD single-phton source. The left/right columns show measurement results before/after conversion, respectively. (a), (b) Optical spectra for the two cases. The QD signal at 917.78 nm in (a) is sent to the frequency converter chip, whose output in (b) consists of the depleted signal and two dominant frequency-shifted idlers (blue idler at 916.17 nm and red idler at 919.39 nm). (c), (d) The intensity autocorrelation of the QD is antibunched ($g^{(2)}(0) < 0.5$) both before and after frequency conversion. Circles are data points and the solid line is a fit to the data. (e), (f) Intensity autocorrelation under pulsed excitation.

The separation between either idler and the depleted QD signal is ≈1.61 nm (≈573.2 GHz) and is equal to the frequency difference between the two 1550 nm pumps, which was set to one free spectral range (FSR) of the microring resonator. The on-chip conversion efficiency is defined as the ratio of the frequency-converted photon flux at the converter chip waveguide output to the input signal-photon flux at the converter chip waveguide input. We estimate the conversion efficiency for the blue idler based on the two spectra [Figs. 3(a) and 3(b)] to be 12.8% ± 1.8%, while photon counting (performed by measuring the photon flux in the input signal band and converted idler band) gives a conversion efficiency value of 11.4% ± 1.6%, where the uncertainties are one standard deviation values due to fluctuations in the detected power and spread in the transmission of optical components in the experimental setup (see Supplement 1 Section III for further discussion). The slightly higher conversion efficiency for the blue idler compared to the red idler is due to its slightly better frequency matching, while the weak higher-order idlers in the spectrum are due to pump mixing and cascaded frequency-conversion effects [37].

The single-photon nature of the QD signal before and after frequency conversion is determined through measurement of its intensity autocorrelation $g^{(2)}(\tau)$ with a standard Hanbury Brown and Twiss setup, where τ is the time delay between detection events on the two detectors. Under continuous-wave (cw) excitation, the QD emits high-purity single photons with $g^{(2)}(0) = 0.080 \pm 0.003$ [Fig. 3(c)]. The one standard deviation uncertainty in $g^{(2)}(0)$ is due to the fluctuation in the count rate on the detectors (Supplement 1 Section IV). After frequency conversion, the blue idler remains antibunched with $g^{(2)}(0) = 0.290 \pm 0.032$; see Fig. 3(d). Thus, the light remains dominantly composed of single photons (relative to multiple photons) [i.e., $g^{(2)}(0) < 0.5$] after frequency conversion. The degradation of the antibunching dip is attributed to resonant noise generated by the 1550 nm pumps, potentially due to Si_3N_4 fluorescence. As discussed later, we operate the frequency converter in a high-pump-power regime to accommodate the relatively large QD linewidth, which comes at the expense of increased noise [37].

The QD becomes a triggered single-photon source when excited by a pulsed laser. The intensity autocorrelation of the QD under pulsed excitation (pulse width = 5 ps and the QD lifetime = 1 ns) is shown in Fig. 3(e). Instead of a complete suppression of coincidences near zero time delay, the correlation curve has a small peak with a dip at zero delay, whose value is used in estimating $g^{(2)}(0) = 0.10 \pm 0.06$. This behavior can likely be attributed to carrier recapture and multiple excitation of the QD within a pump pulse [42,43]. The autocorrelation of the frequency-converted blue idler for pulsed excitation remains antibunched with $g^{(2)}(0) = 0.31 \pm 0.07$ [Fig. 3(f)]. Similar to the cw case, noise from the converter chip results in an increase in $g^{(2)}(0)$, with the level of degradation similar in the two cases. The pulsed measurement enables a clear attribution of the degradation in $g^{(2)}(0)$ to the frequency converter, as its noise is time invariant and therefore not correlated with the QD itself but is instead due to the cw pumps. The impact of converter noise, whose on-chip flux is estimated to be 1.5×10^4 s^{-1} and uniformly distributed in time, can be reduced if the on-chip QD photon flux is increased (e.g., through better coupling efficiency) or if we operate at lower pump powers, which is possible for a narrower-linewidth QD source and will reduce the noise level. Further discussion of the frequency-converter noise is in Supplement 1 Section VIII.

To determine the maximum attainable conversion efficiency if a narrower-linewidth source is available, we substitute the QD source with a ≈200 kHz linewidth cw laser and measure the output of the frequency-conversion chip on an optical spectrum analyzer. Figure 4(a) shows the measured spectrum, where the two prominent sidebands are the blue and red idlers (ω_{i+} and ω_{i-}). In contrast to Fig. 3(b), we observed that the conversion efficiency is significantly higher (≈ 31% versus ≈12% for the blue idler) and the signal (ω_s) has been much more strongly depleted. This suggests that the linewidth of the QD source is the cause of decreased conversion efficiency. In Section IX of Supplement 1, we discuss factors that limit the conversion efficiency to 31%, namely, conversion into multiple idlers rather than a single idler and non-unity outcoupling of converted light into the access waveguide. Correcting for these non-idealities should enable conversion efficiency approaching 90%.

We consider the role of source linewidth on conversion efficiency by scanning the narrow-linewidth input laser across the cavity mode at 917 nm [Fig. 4(b)]. The linear transmission

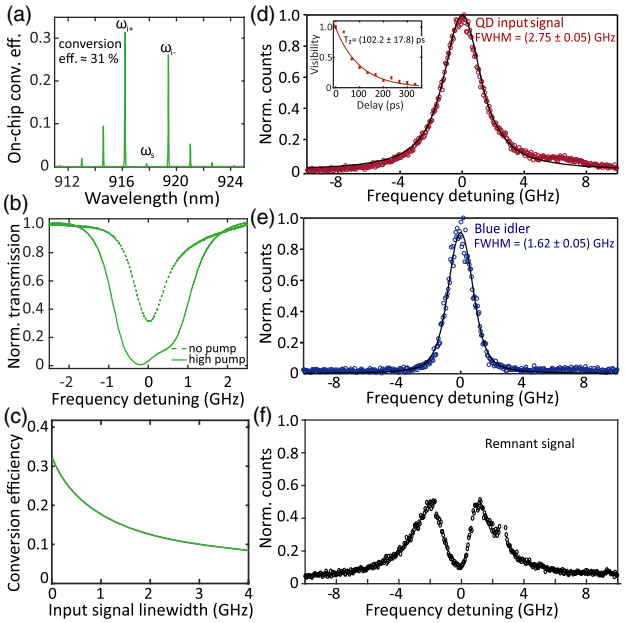

Fig. 4. Influence of QD linewidth on frequency converter performance. (a) The frequency converter output spectrum for a narrow-linewidth cw laser input. (b) Transmission spectrum of the microring frequency converter in the linear regime (with no pumps) and the nonlinear regime (total on-chip pump power ≈20 mW) when scanned by a laser centered at 917 nm, providing an indication of the converter bandwidth. (c) Calculation of the expected conversion efficiency (green curve) as a function of input signal linewidth at a fixed linear linewidth for the microring frequency converter (1.12 GHz) and 1550 nm pump power (20 mW on-chip). (d) Measurement of the QD linewidth before frequency conversion, using a scanning Fabry–Perot resonator. (inset) Measurement of the QD coherence time before frequency conversion, using an unbalanced Mach–Zehnder interferometer, normalized to the visibility at zero delay. The two measurements agree to within their uncertainties, which are one standard deviation values determined from nonlinear least squares fits to functional forms for the spectrum (Voigt) and coherence time (single-sided exponential). (e) Measurement of the frequency-converted blue idler linewidth, which is reduced relative to the linewidth in (d) due to the narrower frequency converter bandwidth. (f) The remnant QD signal (i.e., unconverted light) shows a dip in its spectrum as a result of the frequency conversion process. In (d)–(f), the circles are data points and the solid lines are Lorentzian fits to the data.

spectrum (i.e., without application of the pumps) shows a linewidth of ≈1 GHz, which increases to ≈2 GHz at relatively high pump powers (10 mW per pump). This suggests that the input source linewidth should be significantly narrower than 2 GHz to achieve full conversion efficiency (this is possible for QDs, for which the radiative-limited linewidth is ≈160 MHz for a lifetime of 1 ns). This prescription can be quantified by solving the coupled mode equations for the frequency converter (Supplement 1 Section VII) with knowledge of a few experimentally measured quantities (pump powers and microring intrinsic and coupling quality factors). Figure 4(c) shows the calculated conversion efficiency as a function of the input signal linewidth (green curve), assuming a Lorentzian frequency spectrum and a loaded linear cavity linewidth of 1.12 GHz. We see that the conversion efficiency is reduced by about a factor of 3 when going from a narrow-band input to a linewidth of 3 GHz.

With this guidance from theory, we next measure the QD source linewidth before and after frequency conversion using a scanning Fabry-Perot (SFP) analyzer with a 200 MHz linewidth. Fitting to a Voigt profile, we measure a QD linewidth of ≈2.75 GHz before frequency conversion [Fig. 4(d)] and a coherence time of ≈102 ps [see inset of Fig. 4(d)] using an unbalanced Mach–Zehnder interferometer; the two values are consistent to within our measurement uncertainties. The two measurements are both subjected to the limitation of timing resolution that is slower than the typical spectral diffusion timescales for InAs/GaAs quantum dots [44], so the measured linewidth/coherence times contain the influence of both dephasing and spectral diffusion processes [45,46]. Referring back to the simulated conversion efficiency in Fig. 4(c), for this input signal linewidth a conversion efficiency slightly more than 10% is expected, close to the experimentally observed efficiency in Fig. 2(b). Moreover, because the frequency converter has a narrower linewidth than the input QD photons, the frequency-converted light has a narrower linewidth of ≈1.62 GHz [Fig. 4(e)]. As intuitively expected, the remnant QD signal (i.e., unconverted light) shows a dip in its spectrum [Fig. 4(f)], further indicating the spectral filtering effect of the microresonator frequency converter.

5. VERSATILITY OF THE FREQUENCY CONVERTER

We further consider how our frequency converter can be used in making identical photons from multiple QDs. As the input wavelengths can lie anywhere within the inhomogeneously broadened QD distribution (typically a 10–50 nm spectral window), our converter must have a broad operating wavelength range. Figure 5(a) shows this to be the case, with the conversion efficiency remaining >20% (mean value of 25%) over an exceedingly broad range of wavelengths from 840 to 980 nm (see Supplement 1 Section VI). Here, we use a tunable, narrow-linewidth cw laser as the input to determine the conversion efficiency in the limit of a narrow source linewidth, and the 1550 nm pumps are fixed at a one FSR separation. Measurements are compared against simulations [dashed line in Fig. 5(a)], which account for the measured dispersion parameters of the microring converter but assume fixed values of the microring intrinsic and coupling quality factors equal to those measured for the 917 nm mode. This is not true in practice, as the resonator-waveguide coupling and intrinsic quality factor vary with wavelength, and this is the main source of discrepancy between theory and experiment.

We next consider the achievable spectral translation range. Use of a resonator means that, for a given device, frequency shifts are limited to integer multiples of the resonator FSR, modulo the resonator linewidth. In Fig. 5(b), we assess how the conversion efficiency changes as we vary this integer multiplier, which we measure by keeping the input signal and one pump near 1525 nm fixed and varying the wavelength of the second pump in the C band. Frequency shifts up to 4.5 THz (12.8 nm, corresponding to 8 FSRs) are achieved with conversion efficiency between ≈21% to ≈34%. Measurements again differ from

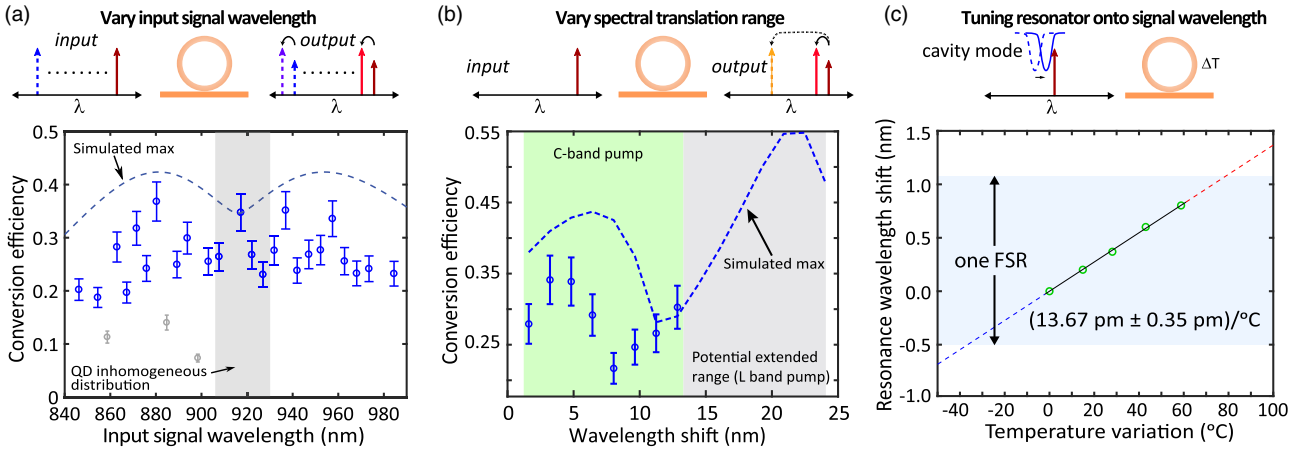

Fig. 5. Versatility of the frequency converter for QD applications. (a) Conversion efficiency (open circles) as the input signal wavelength is varied while keeping the pump separation fixed. Gray data points correspond to wavelengths for which the microring frequency converter exhibits significant frequency mismatch due to mode interaction effects. The dashed curve is the simulated conversion efficiency, assuming experimentally estimated dispersion parameters and the assumption of fixed cavity quality factors. Error bars are one standard deviation uncertainties due to variations in fiber-to-chip coupling efficiency. (b) Conversion efficiency (open circles) as the frequency shift is varied by changing the spectral separation between the two pumps (input signal is fixed). The demonstrated range is limited to 12.8 nm (green shaded area), while a different choice of second pump laser is predicted to increase the range to >22 nm. Circles are data points and the dashed line is a simulated curve. (c) Fine tuning of the nearest microring mode onto resonance with a fixed input signal through temperature. Circles are measured data points, while dashed lines represent an extended temperature range (uncertainties in the measured data are smaller than the symbol size). A linear fit to the data gives a tuning rate of (13.67 pm + 0.35 pm)/°C, where the uncertainty is a 95% confidence interval from the fit.

prediction [dashed line in Fig. 5(b)] due to the assumption of fixed intrinsic and coupling quality factors for resonator modes. We note that the spectral translation range is not limited by the device but instead by the lasers available. Using an L-band laser with coverage up to 1600 nm for the second pump results in predicted spectral shifts in excess of 8 THz (22.4 nm). In addition, the predicted conversion efficiency has significantly gone up. This is due to an increased asymmetry in the degree to which both the blue and red idlers are nearly equally well frequency matched. A strong mismatch for one idler yields a higher conversion efficiency for the better-matched idler, as has been observed in practice in the case of wideband conversion in Ref. [37].

The frequency converter's discrete spectral resonances also require precise spectral matching between the input wavelength and an appropriate microresonator mode. As we have already shown that conversion efficiency is high for modes that span a broad range of input wavelengths [Fig. 5(a)], we simply need to tune the nearest resonator mode to match the input signal. This is done by temperature tuning the microresonator, with any resulting spectral mismatch that occurs in the 1550 nm pump band compensated by tuning the individual pumps while keeping the pump separation fixed so that the temperature tuning does not influence the spectral translation range. Figure 5(c) shows tuning of the microring mode at 917 nm for a temperature change of up to ≈60°C, over which an approximately linear shift of 13.7 pm/°C is observed. The total wavelength shift of ≈820 pm is a bit more than half of the resonator FSR (1.6 nm). Full FSR tuning would ensure that any input signal and a resonator mode could be matched, and it can be achieved through a further increase in the temperature or by cooling, as the thermo-optic coefficient of Si_3N_4 remains nearly constant down to 200 K [47]. Finally, the resonator FSR can be decreased to reduce the fundamental increment of the frequency shift. For our devices, the ring radius (which largely controls the FSR) can be increased without influencing phase/frequency matching (which is largely determined by the ring width and thickness). One can thus envision many different frequency-converter rings on the same chip, or even the same bus waveguide, where the rings differ in radius only, to provide different spectral translation increments.

6. CONCLUSION

In conclusion, we have demonstrated quantum frequency conversion of single photons from a QD using a nanophotonic frequency converter, with an on-chip conversion efficiency (≈12%) primarily limited by the linewidth of the QD source relative to the frequency converter bandwidth. Improved conversion efficiency can be obtained by using QD sources with sufficiently narrow linewidths (ideally a few times smaller than the converter bandwidth) or by increasing the loaded linewidth of the converter (Supplement 1 Section VII). Future directions include demonstration of telecom-band downconversion and heterogeneous integration of the two elements using the approach developed in Ref. [40]. The ability to achieve >90% transfer efficiency of single photons from an InAs/GaAs QD single-photon source and a thick Si_3N_4 waveguiding layer shown in that work, together with the optical compatibility of the QD single-photon source and Si_3N_4 microring frequency converter shown in this work suggests a future route to single-chip integration, a critical step when identical photons from multiple QDs on the same chip are needed.

Funding. NIST–UMD (70NANB10H193); Center for Nanoscale Science and Technology (CNST) (70NANB10H193); Bundesministerium für Bildung und Forschung (BMBF); Deutsche Forschungsgemeinschaft (DFG) (SCHN1376 5.1); National Key R&D Program of China (2018YFA0306100); National Natural Science Foundation of China (NSFC) (11874437, 11704424); Natural Science Foundation of Guang-dong Province (2018B030311027, 2017A030310004, 2016A030310216); Guangzhou Science and Technology Project (201805010004).

Acknowledgment. A. Singh, Q. Li, and X. Lu acknowledge support under the Cooperative Research Agreement between the UMD and NIST-PML. C. Schneider and S. Höfling acknowledge support by the State of Bavaria and the BMBF within the project Q.Com-HL. C. Schneider acknowledges funding by the DFG.

See Supplement 1 for supporting content.

REFERENCES

1. H. J. Kimble, "The quantum internet," Nature **453**, 1023–1030 (2008).
2. T. D. Ladd, F. Jelezko, R. Laflamme, Y. Nakamura, C. Monroe, and J. L. O'Brien, "Quantum computers," Nature **464**, 45–53 (2010).
3. T. E. Northup and R. Blatt, "Quantum information transfer using photons," Nat. Photonics **8**, 356–363 (2014).
4. G. Kurizki, P. Bertet, Y. Kubo, K. Mølmer, D. Petrosyan, P. Rabl, and J. Schmiedmayer, "Quantum technologies with hybrid systems," Proc. Natl. Acad. Sci. USA **112**, 3866–3873 (2015).
5. A. F. Koenderink, A. Alù, and A. Polman, "Nanophotonics: shrinking light-based technology," Science **348**, 516–521 (2015).
6. P. Michler, *Single Semiconductor Quantum Dots* (Springer-Verlag, 2009).
7. I. Aharonovich, D. Englund, and M. Toth, "Solid-state single-photon emitters," Nat. Photonics **10**, 631–641 (2016).
8. P. Senellart, G. Solomon, and A. White, "High-performance semiconductor quantum-dot single-photon sources," Nat. Nanotechnol. **12**, 1026–1039 (2017).
9. N. Somaschi, V. Giesz, L. De Santis, J. C. Loredo, M. P. Almeida, G. Hornecker, S. L. Portalupi, T. Grange, C. Anton, J. Demory, C. Gomez, I. Sagnes, N. D. L. Kimura, A. Lemaitre, A. Auffeves, A. G. White, L. Lanco, and P. Senellart, "Near optimal single photon sources in the solid state," Nat. Photonics **10**, 340–345 (2016).
10. X. Ding, Y. He, Z.-C. Duan, N. Gregersen, M.-C. Chen, S. Unsleber, S. Maier, C. Schneider, M. Kamp, S. Höfling, C.-Y. Lu, and J.-W. Pan, "On-demand single photons with high extraction efficiency and near-unity indistinguishability from a resonantly driven quantum dot in a micropillar," Phys. Rev. Lett. **116**, 020401 (2016).
11. S. Unsleber, Y.-M. He, S. Gerhardt, S. Maier, C.-Y. Lu, J.-W. Pan, N. Gregersen, M. Kamp, C. Schneider, and S. Höfling, "Highly indistinguishable on-demand resonance fluorescence photons from a deterministic quantum dot micropillar device with 74% extraction efficiency," Opt. Express **24**, 8539–8546 (2016).
12. Y.-M. He, J. Liu, S. Maier, M. Emmerling, S. Gerhardt, M. Davanço, K. Srinivasan, C. Schneider, and S. Höfling, "Deterministic implementation of a bright, on-demand single-photon source with near-unity indistinguishability via quantum dot imaging," Optica **4**, 802–808 (2017).
13. P. Kok, W. J. Munro, K. Nemoto, T. C. Ralph, J. P. Dowling, and G. J. Milburn, "Linear optical quantum computing with photonic qubits," Rev. Mod. Phys. **79**, 135–174 (2007).
14. S. Aaronson and A. Arkhipov, "The computational complexity of linear optics," in *ACM Symposium on Theory of Computing*, San Jose, California, 2011, pp. 333–342.
15. B. T. Gard, K. R. Motes, J. P. Olson, P. P. Rohde, and J. P. Dowling, "An introduction to boson-sampling," in *From Atomic to Mesoscale: the Role of Quantum Coherence in Systems of Various Complexities* (World Scientific, 2014), pp. 167–192.

16. J. C. Loredo, M. A. Broome, P. Hilaire, O. Gazzano, I. Sagnes, A. Lemaitre, M. P. Almeida, P. Senellart, and A. G. White, "Boson sampling with single-photon Fock states from a bright solid-state source," Phys. Rev. Lett. **118**, 130503 (2017).
17. Y. He, X. Ding, Z. E. Su, H. L. Huang, J. Qin, C. Wang, S. Unsleber, C. Chen, H. Wang, Y. M. He, X. L. Wang, W. J. Zhang, S. J. Chen, C. Schneider, M. Kamp, L. X. You, Z. Wang, S. Höfling, C. Y. Lu, and J. W. Pan, "Time-bin-encoded Boson sampling with a single-photon device," Phys. Rev. Lett. **118**, 190501 (2017).
18. H. Wang, Y.-M. He, Y. H. Li, Z. E. Su, B. Li, H. L. Huang, X. Ding, M. C. Chen, C. Liu, J. Qin, J. P. Li, Y. M. He, C. Schneider, M. Kamp, C. Z. Peng, S. Höfling, C. Y. Lu, and J. W. Pan, "High-efficiency multiphoton Boson sampling," Nat. Photonics **11**, 361–365 (2017).
19. S. Seidl, M. Kroner, A. Högele, K. Karrai, R. J. Warburton, A. Badolato, and P. M. Petroff, "Effect of uniaxial stress on excitons in a self-assembled quantum dot," Appl. Phys. Lett. **88**, 203113 (2006).
20. R. Bose, D. Sridharan, G. S. Solomon, and E. Waks, "Large optical Stark shifts in semiconductor quantum dots coupled to photonic crystal cavities," Appl. Phys. Lett. **98**, 121109 (2011).
21. F. Findeis, M. Baier, E. Beham, A. Zrenner, and G. Abstreiter, "Photocurrent and photoluminescence of a single self-assembled quantum dot in electric fields," Appl. Phys. Lett. **78**, 2958–2960 (2001).
22. E. B. Flagg, A. Muller, S. V. Polyakov, A. Ling, A. Migdall, and G. S. Solomon, "Interference of single photons from two separate semiconductor quantum dots," Phys. Rev. Lett. **104**, 137401 (2010).
23. R. B. Patel, A. J. Bennett, I. Farrer, C. A. Nicoll, D. A. Ritchie, and A. J. Shields, "Two-photon interference of the emission from electrically tunable remote quantum dots," Nat. Photonics **4**, 632–635 (2010).
24. Y. He, Y.-M. He, Y.-J. Wei, X. Jiang, M.-C. Chen, F.-L. Xiong, Y. Zhao, C. Schneider, M. Kamp, S. Höfling, C.-Y. Lu, and J.-W. Pan, "Indistinguishable tunable single photons emitted by spin-flip Raman transitions in InGaAs quantum dots," Phys. Rev. Lett. **111**, 237403 (2013).
25. A. J. Bennett, R. B. Patel, J. Skiba-Szymanska, C. A. Nicoll, I. Farrer, D. A. Ritchie, and A. J. Shields, "Giant Stark effect in the emission of single semiconductor quantum dots," Appl. Phys. Lett. **97**, 031104 (2010).
26. F. Pagliano, Y. Cho, T. Xia, F. van Otten, R. Johne, and A. Fiore, "Dynamically controlling the emission of single excitons in photonic crystal cavities," Nat. Commun. **5**, 5786 (2014).
27. X. Yuan, F. Weyhausen-Brinkmann, J. Martín-Sánchez, G. Piredda, V. Křápek, Y. Huo, H. Huang, C. Schimpf, O. G. Schmidt, J. Edlinger, G. Bester, R. Trotta, and A. Rastelli, "Uniaxial stress flips the natural quantization axis of a quantum dot for integrated quantum photonics," Nat. Commun. **9**, 3058 (2018).
28. D. Tumanov, N. Vaish, H. A. Nguyen, Y. Curé, J.-M. Gérard, J. Claudon, F. Donatini, and J.-P. Poizat, "Static strain tuning of quantum dots embedded in a photonic wire," Appl. Phys. Lett. **112**, 123102 (2018).
29. P. Kumar, "Quantum frequency conversion," Opt. Lett. **15**, 1476–1478 (1990).
30. M. G. Raymer and K. Srinivasan, "Manipulating the color and shape of single photons," Phys. Today **65**(11), 32–37 (2012).
31. M. T. Rakher, L. Ma, O. Slattery, X. Tang, and K. Srinivasan, "Quantum transduction of telecommunications-band single photons from a quantum dot by frequency upconversion," Nat. Photonics **4**, 786–791 (2010).
32. S. Zaske, A. Lenhard, C. A. Keßler, J. Kettler, C. Hepp, C. Arend, R. Albrecht, W. M. Schulz, M. Jetter, P. Michler, and C. Becher, "Visible-to-telecom quantum frequency conversion of light from a single quantum emitter," Phys. Rev. Lett. **109**, 147404 (2012).
33. K. De Greve, L. Yu, P. L. McMahon, J. S. Pelc, C. M. Natarajan, N. Y. Kim, E. Abe, S. Maier, C. Schneider, M. Kamp, S. Höfling, R. H. Hadfield, A. Forchel, M. M. Fejer, and Y. Yamamoto, "Quantum-dot spin-photon entanglement via frequency downconversion to telecom wavelength," Nature **491**, 421–425 (2012).
34. S. Ates, I. Agha, A. Gulinatti, I. Rech, M. T. Rakher, A. Badolato, and K. Srinivasan, "Two-photon interference using background-free quantum frequency conversion of single photons emitted by an InAs quantum dot," Phys. Rev. Lett. **109**, 147405 (2012).
35. J. H. Weber, B. Kambs, J. Kettler, S. Kern, J. Maisch, H. Vural, M. Jetter, S. L. Portalupi, C. Becher, and P. Michler, "Two-photon interference in the telecom C-band after frequency conversion of photons from remote quantum emitters," Nat. Nanotechnol. **14**, 23–26 (2019).
36. C. McKinstrie, J. Harvey, S. Radic, and M. Raymer, "Translation of quantum states by four-wave mixing in fibers," Opt. Express **13**, 9131–9142 (2005).
37. Q. Li, M. Davanço, and K. Srinivasan, "Efficient and low-noise single-photon-level frequency conversion interfaces using silicon nanophotonics," Nat. Photonics **10**, 406–414 (2016).
38. H. J. McGuinness, M. G. Raymer, C. J. McKinstrie, and S. Radic, "Quantum frequency translation of single-photon states in a photonic crystal fiber," Phys. Rev. Lett. **105**, 093604 (2010).
39. S. Clemmen, A. Farsi, S. Ramelow, and A. L. Gaeta, "Ramsey interference with single photons," Phys. Rev. Lett. **117**, 223601 (2016).
40. M. Davanço, J. Liu, L. Sapienza, C. Z. Zhang, J. V. De Miranda Cardoso, V. Verma, R. Mirin, S. W. Nam, L. Liu, and K. Srinivasan, "Heterogeneous integration for on-chip quantum photonic circuits with single quantum dot devices," Nat. Commun. **8**, 889 (2017).
41. D. J. Moss, R. Morandotti, A. L. Gaeta, and M. Lipson, "New CMOS-compatible platforms based on silicon nitride and Hydex for nonlinear optics," Nat. Photonics **7**, 597–607 (2013).
42. T. Aichele, V. Zwiller, and O. Benson, "Visible single-photon generation from semiconductor quantum dots," New J. Phys. **6**, 90 (2004).
43. A. Singh, P. M. de Roque, G. Calbris, J. T. Hugall, and N. F. van Hulst, "Nanoscale mapping and control of antenna-coupling strength for bright single photon sources," Nano Lett. **18**, 2538–2544 (2018).
44. A. V. Kuhlmann, J. Houel, A. Ludwig, L. Greuter, D. Reuter, A. D. Wieck, M. Poggio, and R. J. Warburton, "Charge noise and spin noise in a semiconductor quantum device," Nat. Phys. **9**, 570–575 (2013).
45. C. Kammerer, G. Cassabois, C. Voisin, M. Perrin, C. Delalande, P. Roussignol, and J. M. Gérard, "Interferometric correlation spectroscopy in single quantum dots," Appl. Phys. Lett. **81**, 2737–2739 (2002).
46. L. Coolen, X. Brokmann, and J. P. Hermier, "Modeling coherence measurements on a spectrally diffusing single-photon emitter," Phys. Rev. A **76**, 033824 (2007).
47. A. W. Elshaari, I. E. Zadeh, K. D. Jöns, and V. Zwiller, "Thermo-optic characterization of silicon nitride resonators for cryogenic photonic circuits," IEEE Photon. J. **8**, 2561622 (2016).